

Electronic relaxation dynamics in large anionic water clusters: $(\text{H}_2\text{O})_n^-$ and $(\text{D}_2\text{O})_n^-$ ($n=25-200$)

Graham B. Griffin,¹ Ryan M. Young,¹ Oli T. Ehrler,¹ and Daniel M. Neumark^{1,2,a)}¹Department of Chemistry, University of California, Berkeley, California 94720, USA²Chemical Sciences Division, Lawrence Berkeley National Laboratory, Berkeley, California 94720, USA

(Received 29 September 2009; accepted 22 October 2009; published online 16 November 2009)

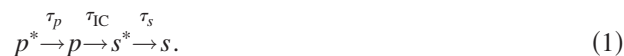
Electronic relaxation dynamics subsequent to $s \rightarrow p$ excitation of the excess electron in large anionic water clusters, $(\text{H}_2\text{O})_n^-$ and $(\text{D}_2\text{O})_n^-$ with $25 \leq n \leq 200$, were investigated using time-resolved photoelectron imaging. Experimental improvements have enabled considerably larger clusters to be probed than in previous work, and the temporal resolution of the instrument has been improved. New trends are seen in the size-dependent p-state lifetimes for clusters with $n \geq 70$, suggesting a significant change in the electron-water interaction for clusters in this size range. Extrapolating the results for these larger clusters to the infinite-size limit yields internal conversion lifetimes τ_{IC} of 60 and 160 fs for electrons dissolved in H_2O and D_2O , respectively. In addition, the time-evolving spectra show evidence for solvent relaxation in the excited electronic state prior to internal conversion and in the ground state subsequent to internal conversion. Relaxation in the excited state appears to occur on a time scale similar to that of internal conversion, while ground state solvent dynamics occur on a ~ 1 ps time scale, in reasonable agreement with previous measurements on water cluster anions and electrons solvated in liquid water. © 2009 American Institute of Physics. [doi:10.1063/1.3263419]

I. INTRODUCTION

The hydrated electron, e_{aq}^- , was first observed by Hart and Boag^{1,2} in 1962 as a broad transient absorption feature appearing around 720 nm following radiolysis of neat water and aqueous salt solutions. Since then, the hydrated electron has emerged as a key species in condensed phase chemistry. From a purely fundamental perspective, it represents the simplest quantum mechanical solute,³ and it plays a key role in radiation chemistry and biology.^{4,5} Many properties of e_{aq}^- are consistent with the “cavity” model, in which this species resides in a solvent cavity with a radius of 2–3 Å.^{6,7} The 720 nm band can then be understood as an $s \rightarrow p$ excitation of the electron within this roughly spherical cavity.^{3,8–10}

There is considerable interest in understanding the mechanism by which hydrated electrons formed by ionization of water relax to their ground state^{11–17} and, more specifically, how these dynamics proceed subsequent to $s \rightarrow p$ excitation.^{18–25} This paper presents new results in our ongoing effort to understand the relaxation dynamics of e_{aq}^- by performing time-resolved experiments on water cluster anions, $(\text{H}_2\text{O})_n^-$, the gas phase analog of the hydrated electron.

In aqueous solution, the relaxation of p-state electrons produced by $s \rightarrow p$ excitation is generally interpreted using the model presented in Fig. 1(a),^{26–28}



In this scheme, p^* and s^* refer to excited and ground electronic state electrons in nonequilibrium solvent configurations formed by optical excitation and internal conversion (IC), respectively, while p and s refer to relaxed solvent configurations in the two electronic states. The time constants τ_p , τ_{IC} , and τ_s refer to excited state solvent relaxation, $p \rightarrow s^*$ IC, and ground state solvent relaxation, respectively.

Transient absorption measurements yield three relaxation time scales: $\tau_1 \approx 30-80$ fs, $\tau_2 \approx 200-300$ fs, and $\tau_3 \approx 1.1$ ps,^{18,21–23} with τ_1 slower in deuterated water by a factor of $\sim 1.4-1.6$.^{18,22} Assignment of these measured time scales to the relaxation processes of Eq. (1) has been controversial. For example, in the “adiabatic” model of hydrated electron dynamics,^{18,21,23,27,29,30} the fastest measured time scale is attributed to solvent relaxation in the excited state ($\tau_1 = \tau_p$), with IC to the ground state occurring on a slower time scale ($\tau_2 = \tau_{\text{IC}}$). The interpretation of the time constants is very different in the “nonadiabatic” model,^{14,22,31} in which the fastest observed relaxation time scale is assigned to IC ($\tau_1 = \tau_{\text{IC}}$), while the slower two time scales are assigned to solvent relaxation in the ground electronic state ($\tau_2 = \tau_s$; $\tau_3 = \tau_{s'}$).

These considerations motivated previous experiments on the time-resolved photoelectron spectroscopy³² (PES) of water cluster anions, $(\text{H}_2\text{O})_n^-$, both in our group^{33,34} and elsewhere.^{35,36} Experiments of this type can directly yield IC lifetimes, in contrast to condensed phase transient absorption measurements, and thus provide a stringent test of the proposed relaxation models for e_{aq}^- .

^{a)}Author to whom correspondence should be addressed. Present address: University of California at Berkeley, B64 Latimer Hall, UC Berkeley, Berkeley CA 94720. Tel.: 510 642 3502. FAX: 510 642 3635. Electronic mail: dneumark@berkeley.edu.

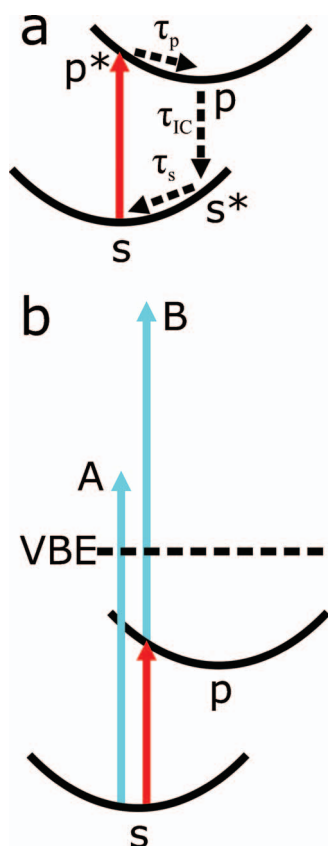


FIG. 1. (a) Diagram of the processes involved in excited state relaxation of the condensed phase hydrated electron. The red arrow represents the pump laser pulse, while black curves represent the *s*-like ground state and *p*-like excited state of the hydrated electron. Various dynamical processes discussed in the text are labeled and diagramed with dashed black arrows. (b) Diagram of the photodetachment processes observed in large anionic water clusters. The black curves show the ground and excited states of the cluster, while the dashed line represents the threshold for vertical detachment. Blue arrows represent the probe laser pulse, while the red arrow represents the pump pulse.

Water cluster anions, $(\text{H}_2\text{O})_n^-$, have been widely studied since they were first observed in 1984,³⁷ in part because they can serve as a model system for the condensed phase hydrated electron.³⁸ These clusters have been studied using many experimental techniques, including electronic spectroscopy,³⁹ one-photon PES,^{40–44} femtosecond time-resolved PES,^{33–36} and infrared photodissociation spectroscopy.^{45–47} These investigations have been both motivated and complemented by numerous theoretical studies of water cluster anion structure and dynamics using quantum path integral methods,^{48–50} electronic structure computations,^{51–56} and both mixed quantum-classical^{57–59} and *ab initio*^{60,61} molecular dynamics calculations. The key results, which have been recently reviewed,^{62,63} are that (i) multiple isomers of water clusters can be formed over a wide size range (up to $n=200$),⁴² (ii) for the isomer that binds the electron most strongly (isomer I), the excess electron is bound by a single unique water molecule at the surface of the cluster up to size $n=25$,⁴⁶ although there is evidence that the electron binding motif changes in larger clusters,⁴⁷ (iii) there is considerable debate about how large a water cluster anion has to be for the excess electron to be internally solvated,^{57,58} and (iv) upon excitation of the $s \rightarrow p$ transition in the cluster

anion, the lifetime of the *p*-state with respect to IC is exceedingly short, extrapolating to $\tau_{\text{IC}}=50$ fs as $n \rightarrow \infty$ for $(\text{H}_2\text{O})_n^-$ clusters.³⁴

Measurements of excited state lifetimes are particularly relevant to the issues addressed in this paper. Results from these experiments can be interpreted in a framework similar to that used in the condensed phase transient absorption measurements, as diagramed in Fig. 1(a). Clusters also have an *s*-like ground state and a *p*-like excited state, and, in principle, can undergo similar dynamical processes (IC and solvent reorganization on both ground and excited states) subsequent to excitation. Early time-resolved experiments by Weber *et al.*,³⁵ on $(\text{H}_2\text{O})_n^-$ clusters with $n=20$ –100 established an upper limit of ~ 150 fs for the lifetime of the excited state. More recently, time-resolved photoelectron imaging experiments by Bragg *et al.*^{33,34} based on the scheme outlined in Fig. 1(b) measured excited state lifetimes in isomer I clusters with $n \leq 50$ (and $n \leq 100$ for deuterated clusters), yielding IC time constants τ_{IC} as fast as ~ 130 fs, for $(\text{H}_2\text{O})_{50}^-$. For clusters with $n \geq 25$, these lifetimes scale linearly with $1/n$ toward a bulk limit of 50 fs (80 fs in deuterated clusters.) Time-resolved PES experiments by Paik *et al.*³⁶ on clusters in the size range of $15 \leq n \leq 35$ revealed electronic relaxation dynamics on time scales of 300 fs and 2–10 ps, which were both attributed to solvent relaxation around the nascent ground state electron following IC.

The extrapolation of IC lifetimes in clusters toward a bulk limit of < 100 fs has been invoked to support the nonadiabatic relaxation model for the bulk hydrated electron.^{33,34} However, given that $(\text{H}_2\text{O})_{50}^-$ was the largest such cluster for which τ_{IC} was measured, studies of dynamics in larger clusters are desirable in order to test the validity of this extrapolation, which has been questioned in recent theoretical work²⁵ on e_{aq}^- . Moreover, experiments with sufficient time resolution to measure τ_p , the time constant for excited state relaxation [see Fig. 1(a)] in clusters, would provide a further point of comparison with condensed phase dynamics. These considerations have motivated the set of experiments on water cluster anions described here, in which improved instrumentation and experimental techniques have enabled us to extend our time-resolved studies to isomer I clusters as large as $n=200$ for both water isotopologs and to measure the associated dynamics with considerably better time resolution than in previous work. The new results show a significant deviation in τ_{IC} from the simple $1/n$ dependence seen previously, and provide clear evidence for both excited state solvent relaxation prior to IC and ground state relaxation subsequent to IC.

II. EXPERIMENT

Our femtosecond time-resolved photoelectron imaging apparatus has been described elsewhere in detail,^{34,64} as have our methods for generating water cluster anions.³⁴ Briefly, Ar backing gas at ~ 20 psi (gauge), seeded with the vapor pressure of water at 30–50 °C, was expanded through a pulsed solenoid valve. A pulsed, ring-shaped ionizer generated anions by secondary electron attachment that are extracted perpendicularly into a Wiley–McLaren⁶⁵ time-of-flight mass

spectrometer. An electrostatic switch allowed only ions of the desired mass-to-charge ratio to pass into the interaction region, where they were intercepted by the excitation (pump) and detachment (probe) laser pulses from a femtosecond laser system. The resulting photoelectrons were projected, in a collinear velocity map imaging⁶⁶ detection scheme, onto a chevron-mounted pair of microchannel plates coupled to a phosphor screen. Images from the phosphor screen were then collected by a charge coupled device camera, and converted into photoelectron spectra using the Basis Set Expansion (BASEX) method.⁶⁷

Clusters larger than $n \approx 100$ were too large for our mass spectrometer to resolve anions differing in mass by a single water molecule since $\Delta m/m \leq 1\%$ in this size range. Hence, results from clusters with $n \geq 100$ we obtained by calibrating the mass spectrometer and using the electrostatic switch to select a section of the continuous cluster distribution. The finite width of the switch gating pulse introduced an uncertainty of $\Delta n = \pm 2$ for both $(\text{H}_2\text{O})_n^-$ and $(\text{D}_2\text{O})_n^-$ clusters. We have previously employed this method in one-photon and time-resolved PES experiments on large water⁶⁸ and methanol^{69,70} clusters.

Femtosecond pump and probe pulses were generated from a Ti:sapphire oscillator/multipass amplifier femtosecond laser system (KM Laboratories Griffin Oscillator/Dragon Amplifier) that produced 3 mJ/pulse at 790 nm when operated at ~ 500 Hz. For clusters larger than $n=50$, 75% of the amplifier output was used to generate the second harmonic at 395 nm (500 μJ /pulse), which served as the probe laser pulse, while the remaining 25% of the amplifier output was further attenuated and used as the pump pulse (790 nm, 80–150 μJ /pulse). In smaller clusters, which do not absorb 790 nm pump pulses efficiently,³⁹ 30% of the amplifier output was used to pump a commercial optical parametric amplifier (TOPAS model 4-800) and the resulting signal output was used as the pump pulse (1250 nm, 15–20 μJ /pulse.) Of the remaining amplifier output, 75% was used to generate the second harmonic probe pulse (395 nm, 400 μJ /pulse) while the remainder was used for alignment purposes.

The peak power of the laser pulses provided by the multipass amplifier was a factor of ~ 10 higher than the regeneratively amplified femtosecond laser system used to perform earlier time-resolved experiments on anionic water clusters.^{33,34} This increase in laser power allowed us to work with larger cluster sizes, for which we generate fewer ions than at smaller sizes. At high pump intensities, however, above-threshold detachment of ground state electrons interfered with observed transient signal in large clusters, requiring attenuation of the pump beam as described above. This attenuation also reduced the contributions to the spectrum from two photon detachment by the pump pulse, which depleted the anion population and interfered with the observed dynamics.

At the amplifier output, the pulses had a 25–35 fs wide [full width at half maximum (FWHM)] Gaussian temporal profile, yielding a ~ 50 fs FWHM Gaussian autocorrelation. The cross correlation of the pump and probe pulses was measured at the laser/ion beam interaction region through detection of the above-threshold detachment signal from large

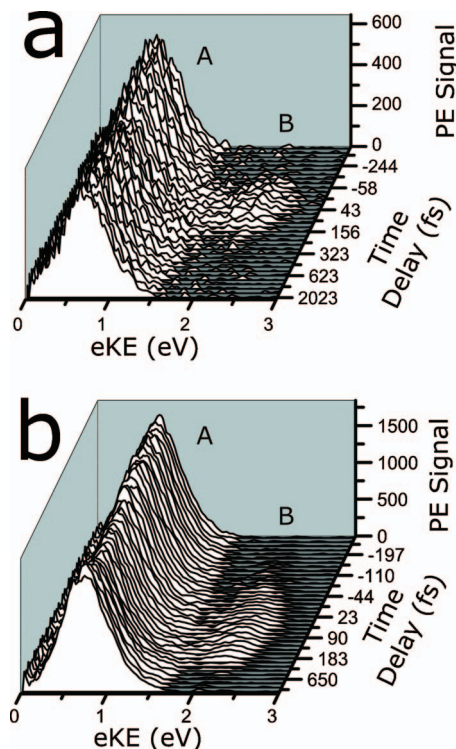


FIG. 2. Time-resolved photoelectron spectra of (a) $(\text{H}_2\text{O})_{150}^-$ and (b) $(\text{D}_2\text{O})_{150}^-$ presented as waterfall plots, with time delay increasing from back to front. Features are labeled A and B with reference to Fig. 1(b).

clusters at high pump intensity; this measurement yielded a Gaussian cross-correlation peak with a width of ~ 100 fs FWHM. Temporal stretching of both laser pulses as they pass through various transmissive optics *en route* to the interaction region accounts for the difference in temporal profile between amplifier output and pulses in the interaction region.

III. RESULTS

Photoelectron spectra were recorded at selected pump-probe time delays ranging from -1.5 to $+2.5$ ps for $(\text{H}_2\text{O})_n^-$ and $(\text{D}_2\text{O})_n^-$ clusters in the size range of $25 \leq n \leq 200$. Additional experiments were performed on $(\text{D}_2\text{O})_n^-$ clusters with $n=40, 80,$ and 120 over a larger delay range, from -2 to $+4$ ps.

Figure 2 shows typical results of these time-resolved photoelectron imaging experiments displayed as waterfall plots of signal versus electron kinetic energy (eKE) with time delay increasing from back to front. Results for $(\text{H}_2\text{O})_{150}^-$ and $(\text{D}_2\text{O})_{150}^-$ are shown in Figs. 2(a) and 2(b), respectively. Each spectrum shows two main features, A (at lower eKE) and B (at higher eKE), which according to Fig. 1(b) and previous results,^{33,34} are assigned to probe-induced detachment from the ground state and pump-probe signal from the excited state, respectively. Other features observed in previous work include autodetachment of clusters excited by the pump pulse and both one and two photon detachments by the pump pulse. These processes are not seen in the spectra presented in Fig. 2, or discussed further in this work, because autodetachment is not observed in clusters

larger than $n=25$, and the pump pulse was attenuated to minimize the effect of one and two photon detachment on the observed dynamics.

For both clusters in Fig. 2, feature B rises rapidly around $t=0$ and decays completely after several hundred femtoseconds. A less obvious effect, particularly in Fig. 2(a), is that feature A is rapidly depleted and then recovers on a time scale similar to the decay of feature B. These effects are seen more clearly when the total signal associated with features A and B is integrated and plotted as a function of delay time, as shown in Fig. 3(a) for $(D_2O)_{150}^-$. These data have been normalized on a 0–1 scale (although feature A is typically depleted by only 5%–15%) and plotted along with associated fit lines, discussed in detail in Sec. IV. Recovery of the ground state feature takes slightly longer than decay of the excited state feature. These results are typical of all cluster sizes studied for both water isotopes.

Figure 3(b) shows the integrated intensity of the excited state feature, along with associated fit lines, for $(D_2O)_{35}^-$, $(D_2O)_{150}^-$, and $(H_2O)_{150}^-$, again normalized on a 0–1 scale for straightforward comparison. All three clusters exhibit qualitatively similar dynamics, increasing in intensity near zero time delay and decaying away with increasing delay. While all three clusters exhibit similar rising edges, the rate of decay varies widely, with $(D_2O)_{150}^-$ decaying faster than $(D_2O)_{35}^-$, and $(H_2O)_{150}^-$ decaying more quickly than either $(D_2O)_n^-$ cluster.

The temporal behavior of features A and B in Fig. 3(a) can be understood with reference to Fig. 1. The initial increase in B and depletion of A reflects pump-induced $s \rightarrow p$ excitation of the cluster. The decay of B represents a p-state decay, while the recovery of A on a similar time scale indicates that the excited state decays by IC, repopulating the s-state of the cluster.

While these effects and their interpretation have been discussed previously, the new results show two more subtle effects discussed in more detail in Secs. IV and V. First, the shape of feature B is not constant with time; its average eKE decreases slightly, typically by ~ 0.1 eV, with increasing pump-probe delay over the lifetime of feature B. Evidence for this effect can be seen in Fig. 3(c), which displays the integrated intensity of three sections of feature B for $(D_2O)_{150}^-$ plotted against time delay, along with connecting lines as a guide to the eye. This plot demonstrates that sections of feature B at higher eKE decay more quickly than at lower eKE. In addition, close inspection of Fig. 3(c) reveals that higher eKE sections of feature B reach peak intensity slightly before lower eKE sections, and that the rising edge of the higher eKE sections is slightly steeper. These observations indicate a shift of feature B intensity toward lower eKE with increasing time delay, consistent with p-state relaxation on a time scale comparable to IC. A similar effect is seen for feature A at longer delay times, reflecting s-state relaxation subsequent to IC.

IV. ANALYSIS

This section presents a quantitative analysis of the results described in Sec. III. The methods used to extract ex-

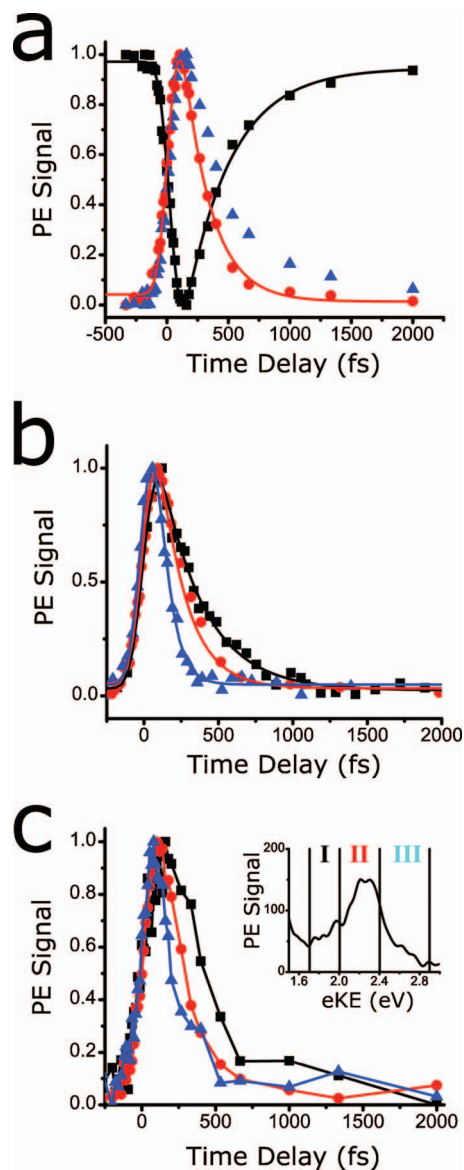


FIG. 3. (a) Integrated intensity of features A (black squares) and B (red circles) at each time delay for $(D_2O)_{150}^-$. Each plot has been normalized on a zero to one scale. Typical data sets exhibit $\sim 5\%$ – 15% maximum depletion of feature A. Best fit lines, as outlined in Sec. IV, are also shown. In addition, the integrated intensity of feature A, normalized on a zero to one scale, is shown inverted (blue triangles) for comparison. (b) Integrated intensities of feature B for $(D_2O)_{35}^-$ (black squares), $(D_2O)_{150}^-$ (red circles), and $(H_2O)_{150}^-$ (blue triangles) are plotted against time delay, normalized on a zero to one scale, along with best fit lines. (c) Integrated intensity of three eKE sections of feature B for $(D_2O)_{150}^-$. The integration range for each section is defined in the inset, with I (black squares) integrated from 1.7 to 2.0 eV, II (red circles) integrated from 2.0 to 2.4 eV, and III (blue triangles) integrated from 2.4 to 2.9 eV. Connecting lines are shown in corresponding color as a guide to the eye.

cited state decay times, ground state recovery times, and eKE shifts in both the excited and ground state features are discussed. Since we are particularly interested in the larger clusters, for which the dynamical time scales are comparable to the laser pulse widths [see Fig. 3(b), for example], these methods are considered in some detail.

The time-dependent integrated intensity of feature B for each cluster is fit to the convolution of an exponential decay/

recovery function and a Gaussian function accounting for the experimental response.⁷¹ Prior to convolution, the exponential decay function has the form

$$I(t) = I_0, \quad t < t_0,$$

$$I(t) = I_0 + A_1 e^{-[t-t_0]/\tau_B}, \quad t \geq t_0, \quad (2)$$

where I_0 is a constant offset accounting for background signal, A_1 is the amplitude of the time-dependent pump-probe signal, and τ_B is the exponential decay time constant. Convolution with the Gaussian experimental response function, centered at t_0 with width defined by standard deviation σ (FWHM = $2\sqrt{2 \ln 2} \sigma$), yields

$$I(t) = I_0 + A_2 \left\{ 1 - \operatorname{erf} \left(\frac{\sigma}{2\tau_B} - \frac{t-t_0}{\sigma} \right) \right\} e^{((\sigma/2 * \tau_B)^2 - [t-t_0]/\tau_B)}, \quad (3)$$

where A_2 is a scaling factor and σ is the standard deviation defining the width of the Gaussian experimental response function. A similar function with recovery time constant τ_A was used to fit feature A.

The data for each cluster could be fit by minimizing χ^2 as a function of the three parameters σ , t_0 , and τ_B in Eq. (3). Using this procedure, we found that the best-fit values of σ varied from day to day with a standard deviation of about 10 fs, a result that more likely reflected the quality of a particular data set rather than actual variations in the instrument response. We thus analyzed the data using the following algorithm. First, global minimum “best fits,” in which τ_B , σ , and t_0 were varied, were obtained for all data sets. Then, the resulting values of σ for all fits were averaged, yielding $\sigma_{\text{av}} \approx 68$ fs, or ~ 160 fs FWHM. Finally, least-squares fitting was performed again on all data sets setting $\sigma = \sigma_{\text{av}}$ but allowing both τ and t_0 to vary when minimizing χ^2 . As mentioned in Sec. II, measurement of above-threshold detachment signal yielded an experimental response function of ~ 100 fs FWHM, somewhat lower than the value obtained from σ_{av} . This discrepancy may indicate that the assumption of an instantaneous rise of $I(t)$ in Eq. (2) is not entirely valid, which could arise from excited state solvation dynamics as discussed in Sec. V B. In any case, the fitting algorithm, which is based on the idea that the actual value of σ does not vary substantially from day to day, yielded more repeatable values of τ_B than fits which allowed τ_B , t_0 , and σ all to vary simultaneously.

Typical fit lines resulting from the fitting described above are shown in both Figs. 3(a) and 3(b). Figure 3(a) shows the results of fitting both the ground and excited state features for $(\text{D}_2\text{O})_{150}^-$, with fitted time constants and associated standard errors of $\tau_A = 372 \pm 23$ and $\tau_B = 223 \pm 11$ fs, respectively. As discussed in Sec. V, the larger value of τ_A may arise from dynamics on the ground state in addition to $p \rightarrow s$ IC. Figure 3(b) shows fit lines yielding time constants of $\tau_B = 290 \pm 15$ fs for $(\text{D}_2\text{O})_{35}^-$, 178 ± 13 fs for $(\text{D}_2\text{O})_{150}^-$, and 79 ± 6 fs for $(\text{H}_2\text{O})_{150}^-$, illustrating the size and isotope dependence of extracted excited state decay dynamics.

The time constants τ_B are displayed in Fig. 4, plotted against $1/n$, at all sizes studied for both $(\text{H}_2\text{O})_n^-$ and $(\text{D}_2\text{O})_n^-$, $25 \leq n \leq 200$. For cluster sizes where multiple ex-

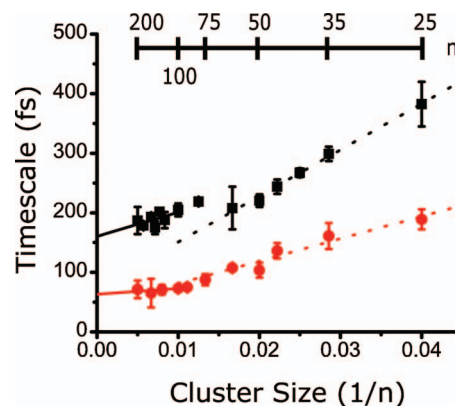


FIG. 4. IC lifetimes, τ_{C} , for $(\text{H}_2\text{O})_n^-$ (red circles) and $(\text{D}_2\text{O})_n^-$ (black squares) plotted against cluster size ($1/n$). Error bars presented represent standard error from averaging of two to three experiments at each cluster size. For cluster sizes where only one experiment was performed, the standard error resulting from the fitting routine is shown. Linear fits of all data points for $n \leq 70$ are shown as dotted lines and for data points with $n > 70$ as solid lines, in red for $(\text{H}_2\text{O})_n^-$ and black for $(\text{D}_2\text{O})_n^-$. The dotted lines have been extended to $1/n = 0.01$ in order to facilitate comparison with the large cluster data.

periments have been performed, the time constants have been averaged at each cluster size. The displayed error bars represent the standard error from this averaging or, for cluster sizes where only one experiment was performed, the standard error in τ_B associated with the least-squares fitting. The resulting error bars range from ± 8 fs for $(\text{D}_2\text{O})_{75}^-$ to ± 38 fs for $(\text{D}_2\text{O})_{25}^-$. Figure 4 represents a key result of our new measurements, as it shows that a simple linear fit of τ_B versus $1/n$ no longer applies when data from larger clusters are included.

Another important result, mentioned in Sec. III, is the shifting of features B and A with time. Figure 5(a) shows the mean eKE of the excited state signal, $\langle \text{eKE} \rangle_{\text{B}}$, along with the total integrated signal of peak B, for $(\text{D}_2\text{O})_{75}^-$. For time delays where the excited state signal is significant, $\langle \text{eKE} \rangle_{\text{B}}$ decreases roughly linearly by about 100 meV over 500 fs. Similar rates are seen for all cluster sizes and both water isotopologs, but the short lifetime of the excited state in these clusters makes it difficult to extract more quantitative detail.

Figure 5(b) shows a similar plot of the mean eKE of the ground state feature, $\langle \text{eKE} \rangle_{\text{A}}$, again plotted along with the integrated intensity of peak B for comparison. This quantity shows a more complicated time dependence. It decreases as excited state population is created, increases sharply as peak B decays, and then, after the excited state population is reduced to zero, decreases by ~ 20 meV over several picoseconds. Experiments were performed over a larger range of time delays for $(\text{D}_2\text{O})_n^-$ with $n = 40, 80,$ and 120 in order to quantify this long-time decrease in $\langle \text{eKE} \rangle_{\text{A}}$. At delays after decay of peak B is complete, fitting the mean eKE of the ground state feature to an exponential of the form

$$\text{eKE}(t) = \text{eKE}_0 + A_3 e^{-t/\tau_{\text{eKE}_A}} \quad (4)$$

yields a time constant $\tau_{\text{eKE}_A} = 1.0 \pm 0.3$ ps for all cluster sizes. As discussed in Sec. V, the shifting features in Figs. 5(a) and 5(b) are attributed to relaxation dynamics on the excited and ground states, respectively. The initial sharp de-

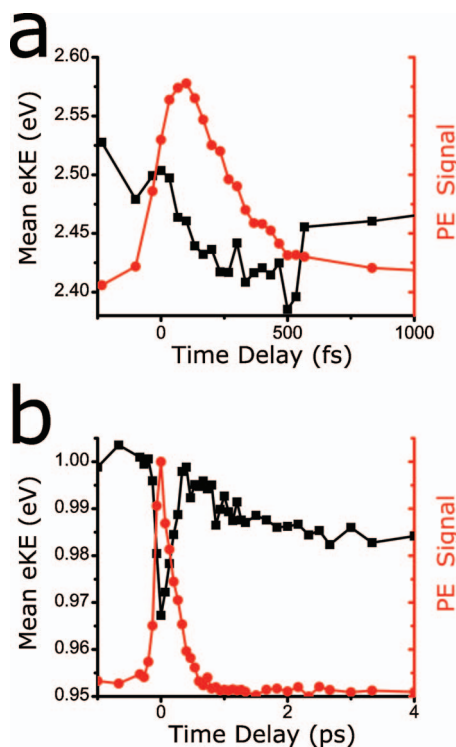


FIG. 5. (a) Mean eKE of feature B ($\langle eKE \rangle_B$, black squares) for $(D_2O)_{75}^-$, along with the integrated intensity of feature B (red circles) plotted against time delay. (b) Mean eKE of feature A ($\langle eKE \rangle_A$, black squares) for $(D_2O)_{80}^-$, along with the integrated intensity of feature B (red circles) plotted against time delay. Connecting lines in both panels are shown in corresponding color as a guide to the eye.

crease and subsequent increase in $\langle eKE \rangle_A$ occur because $s \rightarrow p$ excitation preferentially depletes the high eKE side of feature A. The small difference between $\langle eKE \rangle_A$ at large positive delays and large negative delays shown in Fig. 5(b) varies zero to about -0.02 eV from day to day, and is attributed to preferential depletion of the high eKE side of feature A from two photon detachment by the pump pulse.

V. DISCUSSION

Several new results on the relaxation dynamics of electronically excited water cluster anions have been presented thus far. We have measured excited state lifetimes for $(H_2O)_n^-$ and $(D_2O)_n^-$ clusters as large as $n=200$, thereby considerably extending the range of cluster sizes for which these data are available. As shown in Fig. 4, the previously measured lifetime trends for the smaller clusters do not fit the new results. In addition, the new time-resolved PE spectra reveal time-dependent shifts in the mean eKE of the excited and ground state features. This section considers the implications of these results in the context of previous work on water cluster anions and the condensed phase hydrated electron.

A. Excited state lifetimes

The size-dependent excited state lifetimes τ_B in Fig. 4 represent the key new result from this work. Over the range of cluster sizes studied here, $\tau_B = \tau_{IC}$, the lifetime with respect to IC, since no excited state autodetachment was

observed.³⁴ These lifetimes are plotted as a function of $1/n$, primarily because our previous work^{33,34} showed a linear dependence of τ_{IC} on $1/n$ for clusters with $25 \leq n \leq 100$. This dependence was subsequently rationalized by Fischer⁷² in terms of a long-range nonadiabatic coupling model. Lifetimes for these smaller clusters were measured as part of this study as well, and found to agree with the previous measurements within error bars. However, Fig. 4 shows that the complete set of lifetimes τ_{IC} for clusters up to $n=200$ cannot be fit to a single line when plotted versus $1/n$, and that the lifetimes become much less sensitive to cluster size for $n > 70$. As an example, if the trend established by the smaller clusters was carried through to large cluster sizes, we would expect $\tau_{IC} \approx 125$ fs for $(D_2O)_{150}^-$. The lifetime reported for this cluster in Fig. 4, 193 ± 8 fs, is demonstrably longer.

A linear extrapolation of τ_{IC} for clusters with $n > 70$ toward the infinite cluster size limit, as shown by the solid lines in Fig. 4, yields values of 63 ± 6 fs for $(H_2O)_n^-$ and 160 ± 18 fs for $(D_2O)_n^-$ as $n \rightarrow \infty$. The new value for $(H_2O)_n^-$ clusters within the error bars of the previously reported value, 54 ± 30 fs,³⁴ which was based on linear extrapolation of lifetimes for clusters with $25 \leq n \leq 50$. However, the new value for $(D_2O)_n^-$ is considerably larger than the previously reported extrapolation of 72 ± 22 fs obtained from the smaller clusters. The larger discrepancy for $(D_2O)_n^-$ reflects the abrupt change in slope around $n=70$, as seen in Fig. 4.

We interpret the change in the size-dependence of the τ_{IC} around $n=70$ as evidence that the nature of the electron-water interaction is changing in this size range. Previously, infrared photodissociation spectra⁴⁵⁻⁴⁷ of clusters with $n \leq 50$ have indicated that the nature of electron binding in anionic water clusters changes noticeably in the $25 \leq n \leq 50$ size range. In particular, the sharp infrared feature around 1500 cm^{-1} associated with a unique water molecule (the double acceptor or AA water) binding a diffuse electron at the cluster surface⁴⁵ becomes less prominent above $n=25$ and is substantially broader by $n=50$.⁴⁷ This spectral evolution may signify a transition from the “double acceptor” electron binding motif toward one in which the excess electron interacts with multiple waters. Further support for the idea of transitional behavior in moderately sized anionic water clusters comes from recent *ab initio* molecular dynamics calculations⁶¹ of $(H_2O)_{32}^-$, which show that while an electron starting inside a cluster of this size spontaneously moves to the surface, electron binding fluctuates between the AA binding motif and a binding interaction with multiple water molecules. In this context, the change in the size dependence of the lifetimes presented in Fig. 4 around $n=70$ provides additional evidence for transitional behavior in intermediate-sized water cluster anions. Whether this transition signals internal solvation of the excess electron remains an open question at this point.

The lifetimes presented in Fig. 4 imply an isotope effect of $\tau_{IC,D_2O}/\tau_{IC,H_2O} \approx 2.6$ at the $n \rightarrow \infty$ limit. A similarly large isotope effect of 2.8 ± 0.2 is observed directly at all cluster sizes with $n \geq 70$, so this result is not an artifact of the extrapolation procedure. Interestingly, a smaller isotope effect of 1.9 ± 0.1 is measured in clusters with $n < 70$, in good

agreement with previous measurements.³⁴ Isotope effects of this magnitude, i.e., larger than the factor of the $\sqrt{2}$ ratio of OH/OD vibrational frequencies, might seem unusual, but a semiclassical calculation⁷³ of τ_{IC} for e_{aq}^- based on Fermi's golden rule yielded an isotope effect of 4, although the actual lifetimes differed from those found here (200 and 800 fs). Similar results have been seen in mixed quantum classical molecular dynamics simulations that predict IC lifetimes of 450 and 850 fs in H_2O and D_2O , respectively, resulting in isotope effect of ~ 2 .⁷⁴ Isotope effects of this magnitude are predicted by the "energy gap law" for IC when the energy gap between two molecular electronic states is larger than the frequency of the accepting vibrational mode.^{75,76} This "weak coupling" picture may, however, be overly simplistic for large water cluster anions, where the extremely short lifetimes are suggestive of some type of conical intersection between the s and p states.

The extrapolated τ_{IC} of 63 fs for $(\text{H}_2\text{O})_n^-$ clusters as $n \rightarrow \infty$ is in good agreement with the fastest relaxation time constant of $\tau_1 \approx 30\text{--}80$ fs measured in transient absorption experiments on electrons in aqueous solution.^{18,22} As discussed previously,^{33,34,63} this observation suggests that τ_1 corresponds to τ_{IC} in Eq. (1), thus supporting the nonadiabatic model for relaxation e_{aq}^- . Further support for this idea can be drawn from the fact that IC lifetimes in large $(\text{H}_2\text{O})_n^-$ clusters exhibit lifetimes well under 100 fs, much faster than either of the longer two bulk relaxation time scales ($\tau_2 = 200\text{--}300$ fs and $\tau_3 = 1.1$ ps). Moreover, experiments on hydrated electrons in D_2O show that only τ_1 exhibits a significant isotope effect, increasing by a factor of 1.2–1.6,^{18,22,23} while τ_2 shows no isotope effect. In the adiabatic solvation picture,¹⁸ τ_2 is attributed to τ_{IC} , a possible concern given that both the cluster data and calculations^{73,74} of the excited state lifetime of e_{aq}^- show a strong isotope effect on the IC rate. The most recent calculations^{24,25} on nonadiabatic decay of e_{aq}^- did not explicitly consider isotope effects.

While extrapolation of our original data for $(\text{D}_2\text{O})_n^-$ clusters yielded $\tau_{\text{IC}} = 72$ fs, in excellent agreement with the fastest time constant for bulk D_2O , the newer extrapolated value of 160 fs based on larger cluster sizes is in poorer agreement with the condensed phase experiments. The origin of this discrepancy remains unclear, but we point out that the cluster temperature is estimated at ≤ 200 K, noticeably colder than the room temperature condensed phase experiments. It is possible that the relaxation dynamics in $(\text{D}_2\text{O})_n^-$ clusters are more sensitive to temperature than in $(\text{H}_2\text{O})_n^-$ since cold deuterated clusters are more easily trapped in hydrogen-bonding configurations that differ from those in room temperature bulk water. Time-resolved experiments in which the cluster temperature is actively controlled⁷⁷ could shed considerable light on this issue.

B. Solvation dynamics on the excited and ground states

Figures 5(a) and 3(c) show that the photoelectron signal shifts toward lower eKE during the excited state lifetime. Figure 5(a) shows that $\langle \text{eKE} \rangle_{\text{B}}$ decreases with increasing

time delay for all delays where significant excited state intensity exists, a phenomenon which is observed for all sizes of both water isotopes. Figure 3(c) shows the integrated intensity of three sections of the excited state feature for $(\text{D}_2\text{O})_{150}^-$, demonstrating that higher eKE portions of the excited state feature decay faster than lower eKE sections. In addition, close inspection reveals that higher eKE sections reach their maximum intensity slightly earlier than lower eKE sections and have slightly steeper rising edges. Sequential rise and fall of the three sections of the excited state feature indicate that excited state photoelectron signal is indeed shifting toward lower eKE, as opposed to faster IC from the high eKE parts of the excited state feature causing the faster decay demonstrated in Fig. 3(c). These dynamics are consistent with solvent rearrangement around the nascent excited state, stabilizing the electron and thus binding it more strongly. Note that evaporation of solvent molecules cannot cause the observed dynamics because smaller clusters have lower binding energies, so evaporation of water molecules would cause $\langle \text{eKE} \rangle_{\text{B}}$ to increase rather than decrease. The short lifetime of the excited state relative to the experimental time resolution (~ 100 fs) prevents accurate quantification of the observed dynamics, but it appears that the solvation dynamics must be occurring on a time scale similar to, or faster than, that of IC.

Changes in $\langle \text{eKE} \rangle_{\text{A}}$ with time delay, indicating solvent dynamics on the ground state, are presented in Fig. 5(b). The exponential decrease in $\langle \text{eKE} \rangle_{\text{A}}$ at long delays, which occurs on a time scale of $\tau_{\text{eKE}_A} = 1.0 \pm 0.3$ ps, is the result of solvent motion about the nascent ground state following IC. The solvent network, distorted from its ground state equilibrium geometry by response to the excited state electron, as demonstrated in Figs. 5(a) and 3(c), must rearrange back toward the equilibrium ground state geometry after IC. The observed 1 ps time scale is similar to, although not completely consistent with, the 2–10 ps relaxation time scales reported in previous studies of solvation dynamics in small water clusters.³⁶ The results also compare favorably with the longest relaxation time scale reported in condensed phase transient absorption experiments, $\tau_3 \approx 1$ ps, supporting the assignment of the observed dynamics to solvent motion toward the equilibrium ground state geometry. Again, it is important to note that evaporation of water molecules from the cluster cannot explain the observed dynamics, as the reduced binding energy from a smaller cluster would result in an increase in $\langle \text{eKE} \rangle_{\text{A}}$ with increasing time delay, rather than a decrease. Evaporation should occur eventually since the photon energy exceeds the binding energy of a water molecule to the cluster,⁷⁸ but must take place well after the dynamics observed in these experiments.

These ground state solvation dynamics may also account for the somewhat larger values of τ_{A} compared to τ_{B} referred to in Sec. IV. While τ_{B} depends only on the excited state lifetime, τ_{A} reflects a convolution of the repopulation of the ground state with any solvation dynamics that affect the photodetachment cross section. For example, if the photodetachment cross section increases from its value just after IC as the solvent molecules rearrange around the excess electron, the apparent recovery time of feature A would be slower than

the disappearance of feature B. This effect is related to the spectral evolution of e_{aq}^- owing to ground state relaxation dynamics; in both cases, the wave function of the excess electron is evolving and this affects the associated experimental observable. Similar effects may be associated with excited state solvation. If the photodetachment cross section from the excited state increases from some minimum value immediately after $s \rightarrow p$ excitation, that could explain the observation that the average rise time resulting from the fitting model is larger than the directly measured experimental cross correlation, as discussed in Sec. IV.

Our observation of excited and ground state relaxation, in addition to IC, strengthens the link between cluster studies and the overall picture of condensed phase hydrated electron dynamics, as outlined in Fig. 1(a). We now see dynamical signatures that can be clearly assigned to excited state relaxation, IC, and ground state relaxation. The observation of excited state relaxation in clusters on a time scale comparable to the very fast IC is particularly noteworthy as it addresses one of the issues raised by the nonadiabatic solvation model for e_{aq}^- : if the time constant for IC really is 50 fs, then when does solvent relaxation on the excited state occur? Our results suggest that this process is as fast or even faster than IC, which would make it very difficult to observe in the transient absorption experiments performed to date on e_{aq}^- . Analogous ideas have been proposed in recent theoretical treatments of e_{aq}^- .⁷⁹

VI. CONCLUSIONS

Time-resolved photoelectron imaging experiments have been carried out on $(\text{H}_2\text{O})_n^-$ and $(\text{D}_2\text{O})_n^-$ cluster anions over a considerably larger size range and with better temporal resolution than in previous work. These experiments probe the relaxation dynamics in these clusters subsequent to $s \rightarrow p$ excitation of the excess electron. Experimental improvements have enabled measurements of the p-state lifetime in clusters as large as $n=200$ for both isotopologs. A plot of this lifetime, τ_{IC} , as a function of $1/n$ shows an abrupt reduction in slope for clusters larger than $n \approx 70$. For these larger clusters, a linear extrapolation of τ_{IC} to the infinite-size limit yields 60 fs in $(\text{H}_2\text{O})_n^-$ and 160 fs in $(\text{D}_2\text{O})_n^-$ clusters. The change in slope at $n \approx 70$ suggests a significant change in the electron-water interaction around that cluster size.

The new experiments also revealed evidence for ultrafast p-state relaxation occurring on a time scale faster or comparable to τ_{IC} , as well as ground state relaxation subsequent to IC with a time constant of ~ 1 ps. These solvation dynamics, in combination with the observed ultrafast IC lifetimes, are best understood within the framework of the nonadiabatic mechanism for relaxation of the condensed phase hydrated electron.

ACKNOWLEDGMENTS

This research was supported by the National Science Foundation under Grant No. CHE-0649647. O.T.E. is thankful to the Alexander von Humboldt foundation (Germany) for support through a Feodor Lynen fellowship.

- ¹E. J. Hart and J. W. Boag, *J. Am. Chem. Soc.* **84**, 4090 (1962).
- ²J. W. Boag and E. J. Hart, *Nature (London)* **197**, 45 (1963).
- ³P. J. Rossky and J. Schnitker, *J. Phys. Chem.* **92**, 4277 (1988).
- ⁴D. M. Bartels, A. R. Cook, M. Mudaliar, and C. D. Jonah, *J. Phys. Chem. A* **104**, 1686 (2000).
- ⁵J. Simons, *Acc. Chem. Res.* **39**, 772 (2006).
- ⁶S. Golden and T. R. Tuttle, *J. Chem. Soc., Faraday Trans. 2* **75**, 474 (1979).
- ⁷L. Kevan, *Acc. Chem. Res.* **14**, 138 (1981).
- ⁸M. Boero, M. Parrinello, K. Terakura, T. Ikeshoji, and C. C. Liew, *Phys. Rev. Lett.* **90**, 226403 (2003).
- ⁹L. Turi, G. Hantal, P. J. Rossky, and D. Borgis, *J. Chem. Phys.* **131**, 024119 (2009).
- ¹⁰R. E. Larsen, W. J. Glover, and B. J. Schwartz, *J. Chem. Phys.* **131**, 037101 (2009).
- ¹¹J. M. Wiesenfeld and E. P. Ippen, *Chem. Phys. Lett.* **73**, 47 (1980).
- ¹²A. Migus, Y. Gauduel, J. L. Martin, and A. Antonetti, *Phys. Rev. Lett.* **58**, 1559 (1987).
- ¹³X. L. Shi, F. H. Long, H. Lu, and K. B. Eisenthal, *J. Phys. Chem.* **100**, 11903 (1996).
- ¹⁴A. Hertwig, H. Hippler, A. N. Unterreiner, and P. Vohringer, *Ber. Bunsen-Ges. Phys. Chem.* **102**, 805 (1998).
- ¹⁵R. Laenen, T. Roth, and A. Laubereau, *Phys. Rev. Lett.* **85**, 50 (2000).
- ¹⁶P. Kambhampati, D. H. Son, T. W. Kee, and P. F. Barbara, *J. Phys. Chem. A* **106**, 2374 (2002).
- ¹⁷C. R. Wang and Q. B. Lu, *Angew. Chem., Int. Ed.* **46**, 6316 (2007).
- ¹⁸K. Yokoyama, C. Silva, D. H. Son, P. K. Walhout, and P. F. Barbara, *J. Phys. Chem. A* **102**, 6957 (1998).
- ¹⁹M. F. Emde, A. Baltuska, A. Kummrow, M. S. Pshenichnikov, and D. A. Wiersma, *Phys. Rev. Lett.* **80**, 4645 (1998).
- ²⁰A. Baltuska, M. F. Emde, M. S. Pshenichnikov, and D. A. Wiersma, *J. Phys. Chem. A* **103**, 10065 (1999).
- ²¹M. Assel, R. Laenen, and A. Laubereau, *Chem. Phys. Lett.* **317**, 13 (2000).
- ²²M. S. Pshenichnikov, A. Baltuska, and D. A. Wiersma, *Chem. Phys. Lett.* **389**, 171 (2004).
- ²³A. Thaller, R. Laenen, and A. Laubereau, *Chem. Phys. Lett.* **398**, 459 (2004).
- ²⁴D. Borgis, P. J. Rossky, and L. Turi, *J. Chem. Phys.* **125**, 064501 (2006).
- ²⁵D. Borgis, P. J. Rossky, and L. Turi, *J. Chem. Phys.* **127**, 174508 (2007).
- ²⁶R. B. Barnett, U. Landman, and A. Nitzan, *J. Chem. Phys.* **90**, 4413 (1989).
- ²⁷B. J. Schwartz and P. J. Rossky, *J. Chem. Phys.* **101**, 6917 (1994).
- ²⁸P. O. J. Scherer and S. F. Fischer, *Chem. Phys. Lett.* **421**, 427 (2006).
- ²⁹B. J. Schwartz and P. J. Rossky, *J. Chem. Phys.* **101**, 6902 (1994).
- ³⁰S. Bratos, J. C. Leicknam, D. Borgis, and A. Staib, *Phys. Rev. E* **55**, 7217 (1997).
- ³¹Y. Kimura, J. C. Alfano, P. K. Walhout, and P. F. Barbara, *J. Phys. Chem.* **98**, 3450 (1994).
- ³²A. Stolow, A. E. Bragg, and D. M. Neumark, *Chem. Rev. (Washington, D.C.)* **104**, 1719 (2004).
- ³³A. E. Bragg, J. R. R. Verlet, A. Kammrath, O. Cheshnovsky, and D. M. Neumark, *Science* **306**, 669 (2004).
- ³⁴A. E. Bragg, J. R. R. Verlet, A. Kammrath, O. Cheshnovsky, and D. M. Neumark, *J. Am. Chem. Soc.* **127**, 15283 (2005).
- ³⁵J. M. Weber, J. Kim, E. A. Woronowicz, G. H. Weddle, I. Becker, O. Cheshnovsky, and M. A. Johnson, *Chem. Phys. Lett.* **339**, 337 (2001).
- ³⁶D. H. Paik, I. R. Lee, D. S. Yang, J. S. Baskin, and A. H. Zewail, *Science* **306**, 672 (2004).
- ³⁷H. Haberland, C. Ludewigt, H. G. Schindler, and D. R. Worsnop, *J. Chem. Phys.* **81**, 3742 (1984).
- ³⁸J. V. Coe, *Int. Rev. Phys. Chem.* **20**, 33 (2001).
- ³⁹P. Ayotte and M. A. Johnson, *J. Chem. Phys.* **106**, 811 (1997).
- ⁴⁰J. V. Coe, G. H. Lee, J. G. Eaton, S. T. Arnold, H. W. Sarkas, K. H. Bowen, C. Ludewigt, H. Haberland, and D. R. Worsnop, *J. Chem. Phys.* **92**, 3980 (1990).
- ⁴¹J. Kim, I. Becker, O. Cheshnovsky, and M. A. Johnson, *Chem. Phys. Lett.* **297**, 90 (1998).
- ⁴²J. R. R. Verlet, A. E. Bragg, A. Kammrath, O. Cheshnovsky, and D. M. Neumark, *Science* **307**, 93 (2005).
- ⁴³J. V. Coe, S. T. Arnold, J. G. Eaton, G. H. Lee, and K. H. Bowen, *J. Chem. Phys.* **125**, 014315 (2006).
- ⁴⁴L. Ma, K. Majer, F. Chiro, and B. v. Issendorff, *J. Chem. Phys.* **131**, 144303 (2009).

- ⁴⁵ N. I. Hammer, J. W. Shin, J. M. Headrick, E. G. Diken, J. R. Roscioli, G. H. Weddle, and M. A. Johnson, *Science* **306**, 675 (2004).
- ⁴⁶ J. R. Roscioli, N. I. Hammer, and M. A. Johnson, *J. Phys. Chem. A* **110**, 7517 (2006).
- ⁴⁷ K. R. Asmis, G. Santambrogio, J. Zhou, E. Garand, J. Headrick, D. Goebert, M. A. Johnson, and D. M. Neumark, *J. Chem. Phys.* **126**, 191105 (2007).
- ⁴⁸ R. N. Barnett, U. Landman, C. L. Cleveland, and J. Jortner, *J. Chem. Phys.* **88**, 4421 (1988).
- ⁴⁹ R. N. Barnett, U. Landman, C. L. Cleveland, and J. Jortner, *J. Chem. Phys.* **88**, 4429 (1988).
- ⁵⁰ R. N. Barnett, U. Landman, G. Makov, and A. Nitzan, *J. Chem. Phys.* **93**, 6226 (1990).
- ⁵¹ K. S. Kim, I. J. Park, S. Lee, K. Cho, J. Y. Lee, J. Kim, and J. D. Joannopoulos, *Phys. Rev. Lett.* **76**, 956 (1996).
- ⁵² J. Kim, J. M. Park, K. S. Oh, J. Y. Lee, S. Lee, and K. S. Kim, *J. Chem. Phys.* **106**, 10207 (1997).
- ⁵³ F. Wang and K. D. Jordan, *J. Chem. Phys.* **116**, 6973 (2002).
- ⁵⁴ A. Khan, *J. Chem. Phys.* **121**, 280 (2004).
- ⁵⁵ J. M. Herbert and M. Head-Gordon, *J. Phys. Chem. A* **109**, 5217 (2005).
- ⁵⁶ T. Sommerfeld, A. DeFusco, and K. D. Jordan, *J. Phys. Chem. A* **112**, 11021 (2008).
- ⁵⁷ L. Turi, W. S. Sheu, and P. J. Rossky, *Science* **309**, 914 (2005).
- ⁵⁸ A. Madarasz, P. J. Rossky, and L. Turi, *J. Chem. Phys.* **130**, 124319 (2009).
- ⁵⁹ L. D. Jacobson, C. F. Williams, and J. M. Herbert, *J. Chem. Phys.* **130**, 124115 (2009).
- ⁶⁰ J. M. Herbert and M. Head-Gordon, *Proc. Natl. Acad. Sci. U.S.A.* **103**, 14282 (2006).
- ⁶¹ T. Frigato, J. VandeVondele, B. Schmidt, C. Schutte, and P. Jungwirth, *J. Phys. Chem. A* **112**, 6125 (2008).
- ⁶² O. T. Ehrler and D. M. Neumark, *Acc. Chem. Res.* **42**, 769 (2009).
- ⁶³ D. M. Neumark, *Mol. Phys.* **106**, 2183 (2008).
- ⁶⁴ A. V. Davis, R. Wester, A. E. Bragg, and D. M. Neumark, *J. Chem. Phys.* **118**, 999 (2003).
- ⁶⁵ W. C. Wiley and I. H. McLaren, *Rev. Sci. Instrum.* **26**, 1150 (1955).
- ⁶⁶ A. Eppink and D. H. Parker, *Rev. Sci. Instrum.* **68**, 3477 (1997).
- ⁶⁷ V. Dribinski, A. Ossadtchi, V. A. Mandelshtam, and H. Reisler, *Rev. Sci. Instrum.* **73**, 2634 (2002).
- ⁶⁸ A. Kammrath, J. R. R. Verlet, G. B. Griffin, and D. M. Neumark, *J. Chem. Phys.* **125**, 076101 (2006).
- ⁶⁹ A. Kammrath, G. B. Griffin, J. R. R. Verlet, R. M. Young, and D. M. Neumark, *J. Chem. Phys.* **126**, 244306 (2007).
- ⁷⁰ A. Kammrath, J. R. R. Verlet, G. B. Griffin, and D. M. Neumark, *J. Chem. Phys.* **125**, 171102 (2006).
- ⁷¹ T. E. Dermota, D. P. Hydutsky, N. J. Bianco, and A. W. Castleman, *J. Phys. Chem. A* **109**, 8254 (2005).
- ⁷² S. F. Fischer and W. Dietz, *Z. Phys. Chem.* **221**, 585 (2007).
- ⁷³ E. Neria and A. Nitzan, *J. Chem. Phys.* **99**, 1109 (1993).
- ⁷⁴ B. J. Schwartz and P. J. Rossky, *J. Chem. Phys.* **105**, 6997 (1996).
- ⁷⁵ R. Englman and J. Jortner, *Mol. Phys.* **18**, 145 (1970).
- ⁷⁶ P. Avouris, W. M. Gelbart, and M. A. Elsayed, *Chem. Rev. (Washington, D.C.)* **77**, 793 (1977).
- ⁷⁷ C. Hock, M. Schmidt, R. Kuhnen, C. Bartels, L. Ma, H. Haberland, and B. von Issendorff, *Phys. Rev. Lett.* **103**, 073401 (2009).
- ⁷⁸ L. A. Posey and M. A. Johnson, *J. Chem. Phys.* **89**, 4807 (1988).
- ⁷⁹ A. A. Zharikov and S. F. Fischer, *J. Chem. Phys.* **124**, 054506 (2006).